UNIVERSITY OF TURKU

PEDOT-MnO_2 Based Nanocomposite for Supercapacitor Application

Master's Thesis

Materials Chemistry

Sultana Shamsun Nahar

Supervisors:

Ashwini Jadhav

Dr. Plawan Jha

Prof. Carita Kvarnström

July 2025

Turku

The originality of this thesis has been checked in accordance with the University of Turku quality assurance system using the Turnitin Originality Check service.

Master of Science in Chemistry Thesis
Department of chemistry, Faculty of Science
University of Turku

Subject: Materials Chemistry
Author: Sultana Shamsun Nahar
Title: PEDOT-MnO_2 Based Nanocomposite for Supercapacitor Application
Supervisors: Ashwini Jadhav, Dr. Plawan Jha, Prof. Carita Kvarnström
Number of pages: 32 pages
Date: July 2025

Key objective of this study was to develop a high-performance electrode material by integrating a conductive polymer (PEDOT) and a transition metal oxide (MnO_2). Individual MnO_2 and PEDOT electrodes were synthesized as well, to compare the electrochemical behavior of the composite. Herein, we have used an anionic surfactant, sodium dodecyl sulfate (SDS) to enhance the surface morphology of individual MnO_2, PEDOT and PEDOT-MnO_2 based nanocomposites. 1 M Na_2SO_4 was used as an electrolyte in a three-electrode setup to perform the electrochemical characterizations. For the electrochemical setup, Ag/AgCl was used as a reference electrode, and graphite foil acts both as working electrode (WE), and counter electrode (CE). The electro-polymerization process was carried out in a potential window of 0 to 1 V with 20 cycles, and a scan rate of 50mV/s using cyclic voltammogram (CV). To reveal the chemical structure, bonding interaction, and surface morphology Raman spectroscopy, FTIR spectroscopy and scanning electron microscopy (SEM) was done respectively. Cyclic voltammetry (CV), galvanostatic charge-discharge (GCD), electrochemical impedance spectroscopy (EIS), employed to find out the electrochemical properties. In this work, the specific capacitance of the nanocomposite was 222 mF/cm^2, the capacitance retention value was 65%, and after 1000 cycles, it achieved this stable capacitance retention. Therefore, all these characterizations performed in this work indicate that the synergistic combination of PEDOT and MnO_2 can improve the capacitive behavior and can be utilized in supercapacitor-type energy storage applications.

Key words: Supercapacitor, PEDOT, MnO_2, electrochemical process

Table of Contents:

1. Introduction	**5**
1.1. Energy storage devices	**6**
1.2. Supercapacitor	**8**
1.3. Application	**14**
1.4. Conductive polymer (PEDOT)	**15**
1.5. Transition metal oxide (MnO_2)	**16**
1.6. Anionic surfactant (SDS)	**17**
2. Experimental	**18**
2.1. Literature review	**18**
2.2. Purpose of the work	**19**
2.3. Materials	**19**
2.4. Synthesis of electrodes	**19**
2.5. General characterization	**21**
2.6. Electrochemical characterization	**22**
3. Result and discussion	**23**
3.1. Raman spectroscopy	**23**
3.2. FTIR analysis	**24**
3.3. SEM analysis	**25**
3.4. Impact of SDS on electro-polymerization	**25**
3.5. Electrochemical behavior	**25**
3.5.1. Cyclic voltammetry (CV)	**25**
3.5.2. Galvanostatic charge-discharge (GCD)	**27**
3.5.3. Electrical impedance spectroscopy (EIS)	**28**
3.5.4. Specific capacitance	**29**
3.5.5. Cycling stability	**31**
3.5.6. Effect of electrolytes	**32**
4. Future prospects	**32**
5. Conclusion	**33**

6. Acknowledgment **33**

7. References **34**

Abbreviation List

CO_2	Carbon dioxide
SC	Supercapacitor
EDLC	Electrochemical double layer capacitor
PSC	Pseudo capacitor
HC	Hybrid capacitor
CV	Cyclic Voltammetry
WE	Working electrode
RE	Reference electrode
CE	Counter electrode
ESR	Equivalent series resistance
HESS	Hybrid energy storage system
GF	Graphite foil

1. Introduction:

Since the industrial revolution, energy production has had a significant influence on modern world. With the swift growth of the industrial economy, living standards have risen in society. For modern energy systems, more than 80% of global energy requirements are fulfilled by fossil fuels. This non-renewable energy resource includes natural gas, oil, coal, etc. Excellent energy density and adaptability, are two important characteristics that make fossil fuels inevitable in manufacturing, electricity production, and especially in the transportation sector. [**1**]

Even though fossil fuel plays a significant role in global development, but there is no way to ignore their unsustainable and acute impact on the environment. For instance, burning fossil fuels is a major source of CO_2 emissions. CO_2, known as a greenhouse gas (GHG), is the primary cause of global warming. According to a statistic, industries such as transportation and electricity (which use fossil fuels) have a significant impact on climate change. Around 16% of GHG emissions come from the transportation sector. Besides, about 31% of GHG are emitted from the electricity production sector. [**2**] The combined impact of GHG emissions led to an increase in the overall global temperature by 1.1°C, which is enough to melt glaciers and raise sea levels. As a result, weather causes frequent natural disasters and makes disturbances in standard ecological systems.

To avoid the catastrophic impact of climate change, most countries came into an agreement. One of the well-known initiatives worldwide is the Paris Agreement. The purpose of this agreement is to minimize GHG emissions and move towards a low-carbon energy economy. In addition, the International Council on clean transportation has set a strategy, Vision 2050. This framework aimed to decarbonize the global transport sector. This initiative includes increasing the performance of vehicles through electrification and employing alternative, sustainable fuels like renewable energy. [**3**] Solar, wind, geothermal, tidal, hydropower, biomass, and nuclear are currently existing renewable energy sources. Renewable energy fulfilled almost 38% of global energy demand in 2024. [**1**] A 2022 statistic estimated that over 520 billion USD was saved by using renewable energy instead of fossil fuels. Not only does this energy source have a substantial positive impact on the economy, but it also has a positive impact on human health, and the environment. For example, using renewable energy in electric vehicles can reduce GHG emissions and prevent air pollution. According to the World Health Organization, millions of premature deaths can be avoided by reducing the air pollution. [**3**]

Despite having these advantages, several obstacles exist in the energy production from renewable sources. As long as the fuel supply is working well, some sources can generate power continuously. Geothermal, hydroelectric, biomass, and nuclear are some examples of sustainable renewable energy sources. However, due to several restrictions, these types of plants need a specific location. For instance, a nuclear power plant is typically built along the shore, because it needs to maintain a cooling system to prevent extreme heat. An enormous volume of water is required for this process. Approximately 5000 meters beneath the surface, where the geothermal vents are located, is a perfect location for a geothermal plant. Additionally, rivers with rapid currents are ideal locations for hydroelectric plants. Seasonal energy sources (solar, tidal, wind) face some challenges in energy storage mechanisms as well. For example, lack of sunlight can prevent the continuous energy production by solar cells. For these reasons, a significant amount of energy is

wasted every day, and power production cannot be aligned with consumption. To mitigate this loss, researchers have focused on developing energy storage systems, like as batteries and supercapacitors. [**4**]

1.1. Energy storage devices:

Rechargeable batteries have sophisticated and technologically advanced characteristics that make them suitable for use in energy storage, vehicles, laptops, medical equipment, smartphones, and other applications. Despite having high energy density; longer charging times, shorter cycle life, and low power densities are some drawbacks of conventional batteries. They also have other challenges, such as environmental safety and thermal management. To address these problems, supercapacitors have emerged as a promising alternative energy storage device. [**5**]

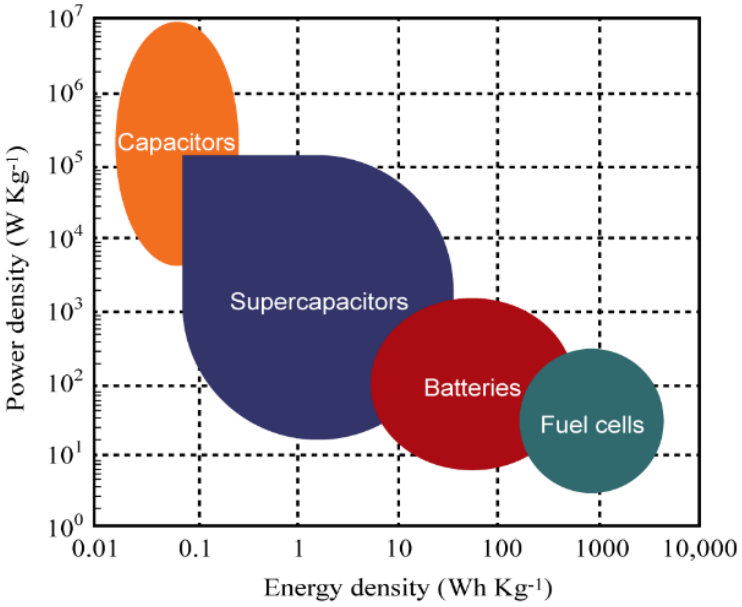

Figure 1: Ragone plot for electrochemical energy storage devices

A comparison of power density and energy density of different energy storage devices shows in **figure 1** with a Ragone plot. A supercapacitor (SC) can bridge the gap between an ordinary capacitor and a battery, owing to its high-power density and moderate energy density. Therefore, it can be an optimal choice over other energy storage systems. Extended lifespan through multiple charge cycles, fast recharging and power delivery capabilities are some of the distinctive characteristics of a supercapacitor. It can operate in a broad range of temperatures, so producing heat does not pose an issue, which makes it a safer alternative to batteries. Therefore, superior power density (>10kW Kg^{-1}), rapid charge-discharge capabilities, extended lifespan, minimal operational expense, and enhanced safety are the beneficial characteristics of supercapacitors that make them special among other energy storage devices. [**6, 7**] With two electrodes, a separator

and electrolyte, a supercapacitor has almost the same structural design as a battery (**Figure 2**). The key difference between battery and SC is shown in **Table 1**.

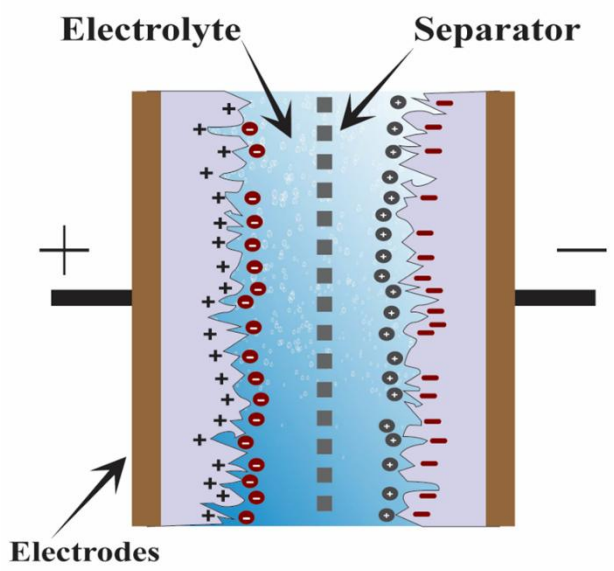

Figure 2: Schematic diagram of SC and battery's general structure

Table 1: Key difference between battery and SC:

Features	Battery	Supercapacitor
Reaction	Chemical	Electrostatic
Energy Density	High	Low
Power Density	Low to moderate	Very high
Charge Time	Slow	Very fast
Cycle Life	Limited (hundreds to thousands of cycles)	Very long (up to millions of cycles)

Among the energy storage devices, the capacitor is another well-known device. It has two metal plates and a dielectric medium as a separator. It is an insulating material, similar to glass, air, plastic and ceramic. It cannot conduct electricity. Upon applying the voltage, electrons begin to

flow from one metal plate to another. When one plate accumulates a negative charge, the other becomes positively charge. Here, the dielectric interrupts the direct flow of charges and forms an electrostatic field. This is the reason a capacitor can store energy. **Figure 3** shows the general schematic diagram of a conventional capacitor. The primary difference between the SC and a conventional capacitor lies in the separator and electrolyte. Instead of dielectric media, SC has a thin insulator as a separator, and SC also has an electrolyte. [**8**]

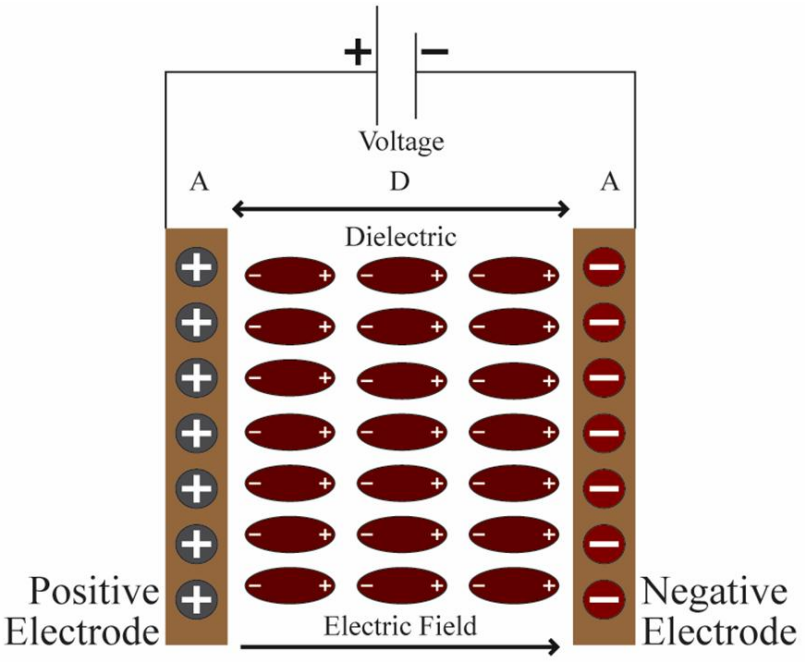

Figure 3: Schematic diagram of an ordinary capacitor

1.2. Supercapacitor:

A SC is divided into three categories: electrochemical double layer capacitor (EDLC), pseudo capacitor (PSC), and hybrid capacitor (HC). All SCs have the same configuration, consisting of two electrodes, an ion-permeable membrane as a separator, and an electrolyte. However, they differ in their reaction mechanisms for storing charge. In EDLC, electrical energy is stored by a non-faradaic mechanism, where the Helmholtz double layer is created (**Figure 4**). [**8**]. When a voltage is applied to the electrodes immersed in a solution, an electric current flows, and the electrodes accumulate charges on their surface. On the other hand, the surrounding solution also develops the equal and opposite charges.

$q^m = - q^s$

Here, q^m indicates the charges of electrode and q^s indicates the charges of solution.

Due to an electrostatic attraction, the other electrode also has the same interactions. The layer that forms due to this interaction is called the Helmholtz double layer. [**9**] Numerous variables,

including electrolyte type, solvent type, electrode type, electrode area, applied voltage, can influence the mechanism and capacity of EDLC. [7]

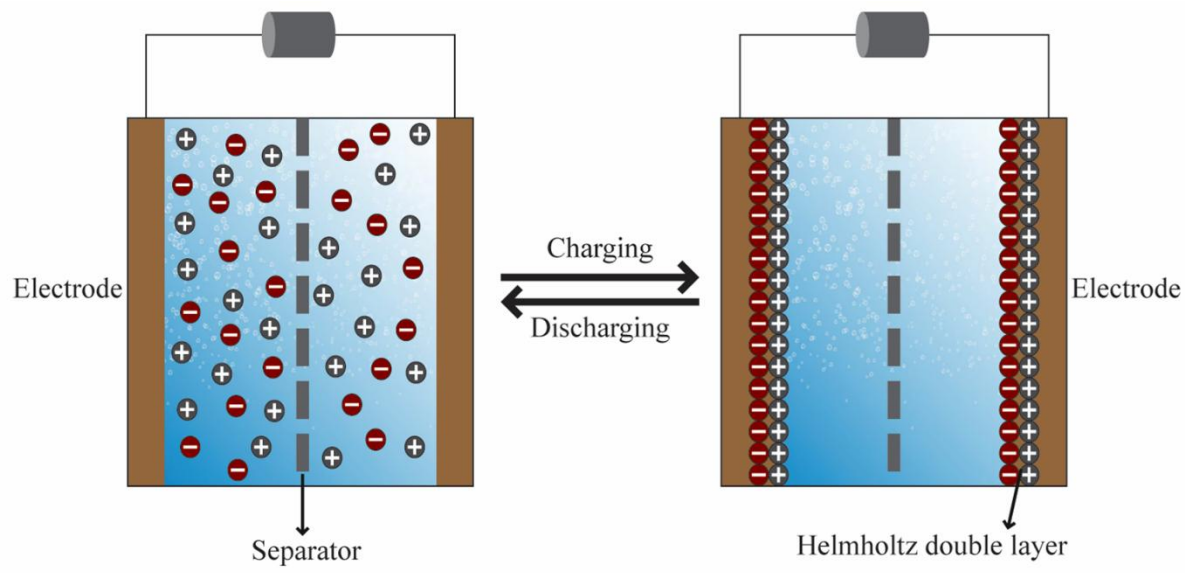

Figure 4: Schematic diagram of charge storage mechanism for EDLC

To analyze the electrochemical performance, cyclic voltammetry (CV) and galvanostatic charge-discharge (GCD) techniques can be used. In this analysis, each mechanism gives a distinctive characteristic shape. For example, EDLC exhibits a rectangular shape in its CV curve (**Figure 5a**), indicating charge accumulation at the electrode-electrolyte interface. It also suggests an ideal capacitive behavior, except for any redox reaction. The GCD curve in the EDLC mechanism (**Figure 5b**) shows a linear triangular shape, which confirms the constant capacitance. [7]

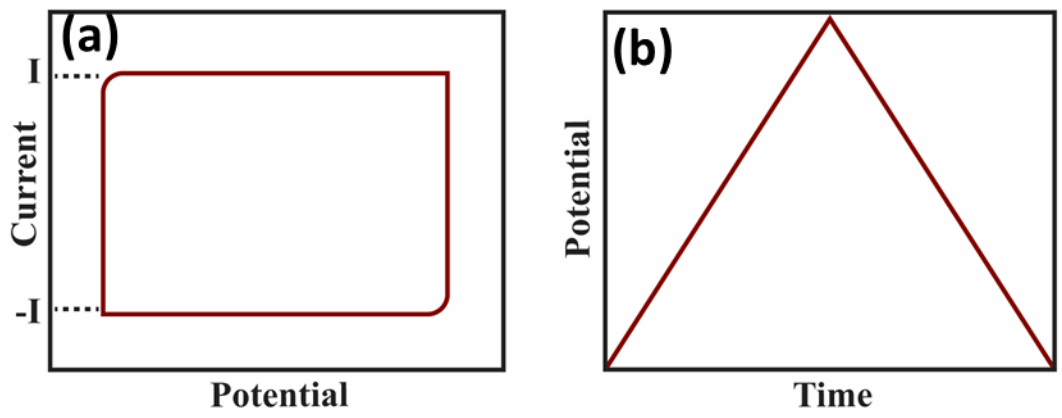

Figure 5: CV (a) and GCD (b) curve of EDLC type SC

In PSC, electrical energy is stored based on a faradic reaction (**Figure 6**), which is a reduction or oxidation reaction of the active material and/or the electrolyte at the electrode-electrolyte interface. Here, electron charge transfer between the electrode and electrolyte enables the electrodes to host fast redox reactions that aid in the electrochemical storage of energy. Redox reaction, electro-

sorption or adsorption, and intercalation are the three electrochemical processes involved in this charge transfer process. [7]

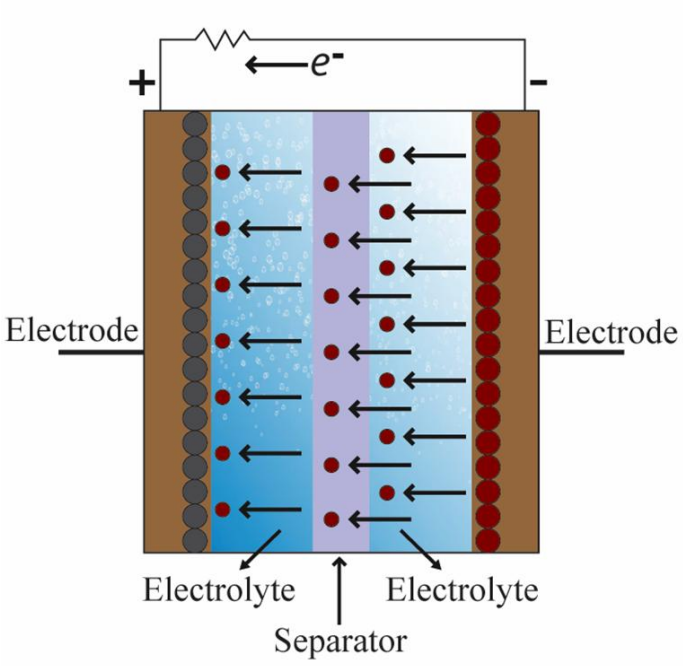

Figure 6: Schematic diagram of charge storage mechanism for PSC

A rapid redox reaction occurs between the electrochemically absorbed ions and the electrode material. When on the electrode, the adsorption and desorption of electrolyte ions occur, resulting in an electro-sorption or adsorption process. Through the van der walls gap, if electrolyte ions enter the electrode lattice, it causes the intercalation process. Except for any chemical or phase transmission reaction, PSC only involves in charge transfer at the electrode-electrolyte surface. As a result, PSC exhibits a quasi-rectangular shape in the CV characterization curve (**Figure 7a**). The GCD curve is also slightly distorted from the ideal triangular shape, which emphasizes on the faradic reaction of the charge storage mechanism (**Figure 7b**). [7] **Table 2** lists all the key differences between EDLC and PSC.

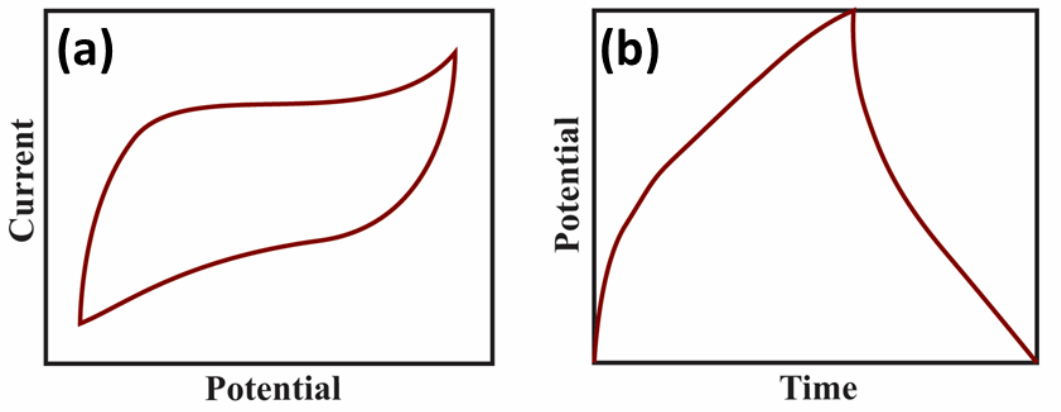

Figure 7: CV (a) and GCD (b) curve of PSC type SC

Table 2: Key difference between EDLC and PSC:

Features	EDLC	PSC
Reaction	Non-faradic/electrostatic	Faradic
Energy storage mechanism	Formation of Helmholtz double layer	Fast reversible redox reaction
Advantages	Excellent electrical conductivity, and cycling stability	Excellent specific capacitance, and energy density
Disadvantages	Poor energy density, and specific capacitance	Poor electrical conductivity and cycling stability
Application	Fast backup power	Higher energy storage

The third type of SC is the hybrid supercapacitor (**Figure 8**), which displays both EDLC and PSC characteristics. This is achieved through the use of materials that demonstrate both types of charge storage mechanisms. The HC incorporates redox faradic and non-faradic reactions to achieve its dual capabilities. Compared to an individual EDLC or PSC, they typically demonstrate a significant range of potential windows and higher capacitance. HC can have asymmetric assembly, depending on the arrangement of electrodes. Asymmetric and symmetric are two configuration types of electrochemical cells. Electrodes in a symmetric assembly will be the same components, whereas different types will form an asymmetric assembly. [**7**]

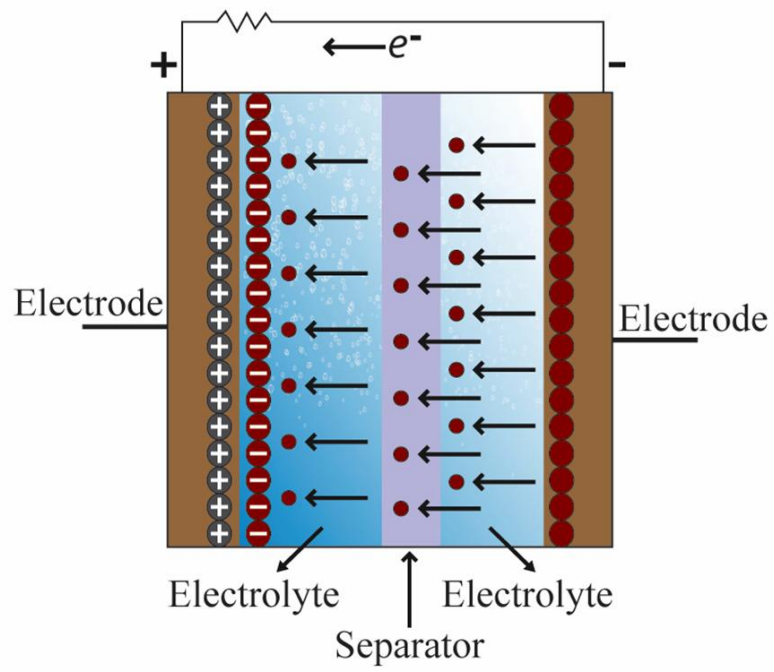

Figure 8: Schematic diagram of charge storage mechanism for HC

A SC has three critical components in its configuration: electrodes, electrolyte, and separator (**Figure 2**). The electrode stands as the most vital component of an electrochemical cell (**Figure 9**), and can be classified into three parts: Reference electrode (RE), counter electrode (CE), and working electrode (WE). The reaction of interest occurs at the WE, which commonly acts as the cathode. When the current direction keeps changing during specific experiments, WE and CE switch their roles as anode and cathode. [**10**] To precisely measure the applied potential, RE is used, which occurs during the current circulation between WE and CE. [**11**]

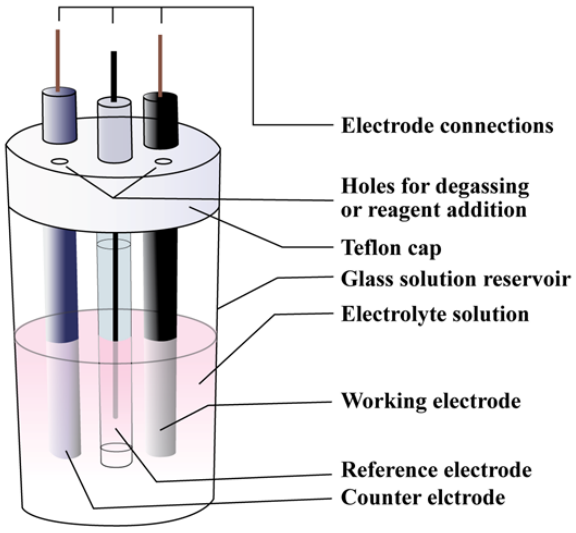

Figure 9: Schematic diagram of an electrochemical cell

RE is also known as a quasi-reference electrode, and "Vs a particular reference" is the standard way to write the applied potential of RE. In a three-electrode setup electrochemical cell, RE is used to measure the applied potential when the current flows between WE and CE. The Ag/AgCl electrode, saturated calomel electrode (SCE), and standard hydrogen electrode (SHE) are typically used as reference electrodes. [**11**] The experimental circumstances that can influence the selection of a reference electrode are the applied current, composition or nature of the electrolyte, and temperature. [**10**]

Current is measured when it starts to flow between the WE and CE. It happens due to an oxidation reaction upon applying a potential to the working electrode. Here, completing the circuit is the primary objective of using the CE, which is also referred to as the auxiliary electrode. Compared to the WE, CE exhibits a larger surface area. A carbon-based electrode or a Pt wire is usually employed as the CE. [**11**]

When a thin layer of active material is deposited on a conductive current collector, it is called WE. The performance of WE can be influenced by several aspects. The reaction kinetics can be accelerated by the porosity and high surface area. Charge transfer impedance, or the reduction of resistance, can enhance electrical conductivity. To increase cycle stability, materials must have thermodynamic, chemical, and high-temperature stability. To ensure effective interactions between the electrolyte and electrode, an optimal surface wettability is essential. To achieve more active sites and enhanced charge storage capacity, the ability to adjust morphology through various nanostructures is necessary. [**6**]

Highly conductive materials with an enhanced surface area are usually required for EDLC-type SCs. Due to having extensive surface area and significant compressibility, carbon-based materials (e.g., graphene compounds, carbon nanotubes, activated carbons, etc.) are usually used in EDLC-type SC. With a rapid charge-discharge rate, EDLC-type SCs can increase cycle stability up to 1 million (10^6) cycles. This happens because it has non-faradic reactions, meaning it does not rely on chemical reactions to store energy. In contrast, redox-active materials are required as the WE for PSC. Due to their low equivalent series resistance (ESR), excellent capacitance, and reversibility, the most widely used WE materials for PSCs are sulfides, nitrides, and transition metal oxides. [**7**]

In an electrochemical cell configuration, the number of charges transferred between the electrodes by the electrolyte can determine the efficiency of the SC. [**12**] Two factors of electrolytes can impact on the efficiency of SC – ionic conductivity and voltage window. The ionic conductivity of the electrolyte can impact power density. If the ions movement is easy in the electrolyte, then SC can deliver more power. To determine the energy density, the voltage window plays an important role. Thermodynamic stability and chemical kinetics of electrolytes can influence this voltage window. [**13**]

A solution of salt, acid, or base with a particular solvent is called an electrolyte. To enhance charge storage performance, the electrolyte can influence the electrodes. Electrolytes are mainly divided into three categories: liquid, solid-state or quasi-solid-state, and redox-active electrolytes. Liquid

electrolytes are again divided into two subsections – aqueous and non-aqueous. Acid, base and neutral are the three categories of aqueous electrolytes. Acidic electrolytes include – H_2SO_4, HCl, K_2SO_4, KCl. Among these electrolytes, H_2SO_4 is the most common one. Many acidic electrolytes are not effective in testing precious metal oxides like Eu, Ni, and Cu. So, basic electrolytes are preferably used there. The most widely used alkaline electrolytes include NaOH, LiOH, and KOH. The third type of aqueous electrolyte is a neutral electrolyte, which includes Na_2SO_4. [**14**]

The separator is another important part of the SC configuration. It can be a highly porous membrane, which permits the flow of electrolyte ions between the two electrodes. It can also serve as an insulator by preventing the electrodes from touching each other. As a result, any kind of incident, such as self-discharging or short-circuiting, can be eliminated. During the operational process, it cannot engage or disrupt the electrochemical reaction occurring between the electrolyte and electrodes; this makes the membrane chemically inert and stable. [**16**] It is also thermally stable, due to its heat tolerance and non-flammability characteristics. [**16**] Polymers, fiberglass textiles, and paper or cellulose can be used as separators. [**17**]

1.3. Application:

In manufacturing companies, the application of supercapacitors has increased recently. It can be used individually or paired with other devices to work efficiently. Large machines like forklifts, cranes, excavators, agricultural machinery use SCs for their operation. High power outputs, exceptional reliability, and rapid charge-discharge duration make SCs more popular among energy storage systems. [**5**]

To prevent the fluctuating power production of renewable energy systems, batteries are combined with SC. This combination is referred to as a hybrid energy storage system (HESS). In the field of renewable energy (which includes wind, tidal, and solar energy), it can be a solution for energy harvesting and distribution functions. SCs used in HESS can reduce the stress and cost of the battery by assisting with load levelling, ensuring smooth power delivery, and contributing to peak power shaving. These functions of HESS can extend the lifespan of a battery. [**4**]

Batteries in electric vehicles can be damaged by abruptly using energy. The quick fluctuations in power consumption can be influenced by several factors, including road condition and driving style. For example, during acceleration, the battery is unable to fulfil the sudden power demand by rapid discharging. This also happens during braking because electric vehicle brakes can produce a current which is stored in the battery. But the battery's lifespan can be reduced by frequent acceleration and braking. Here, HESS can be a better solution because, during deceleration, it can store the brake energy. To accelerate the vehicle, SC uses this energy. Whereas, to operate electronics within the car, air conditioning, and heating the car battery uses this energy. [**18**]

Recent advancements have led to the introduction of micro-supercapacitors and flexible supercapacitors. These types of SC can be used in wearable electronics. There are several types of leading companies working on portable electronic devices, consumer products,

telecommunications, and information technology that are interested in producing these types of SC. For instance, CAP-XX Limited and Nokia Corporation. [**5**]

Furthermore, it can be used in numerous sectors, including artificial intelligence, robotics, sensors, healthcare, and airline emergency exits, etc. Due to its lightweight and dealing capability with extensive temperatures ranging from 40 to 150 °C, SC can be a perfect fit for military vehicles, electromagnetic pulse weapons, radar systems, missiles, communication equipment, and military microgrids, etc. [**4**, **5**]

1.4. Conductive Polymer (PEDOT):

Conductive polymers are organic polymers that can conduct electricity. They have gained significant attention from researchers as advanced materials of the 21st century. [**19**] Their simple synthesis process, structural flexibility, and high electrical conductivity are notable advantages. Their conjugated molecular structure, which includes alternating single and double bonds along the polymer backbone, is the reason for their electrical conductivity. This conjugated structure enables the delocalization of π-electrons, which enhances charge transfer. Because of this structural characteristic, it is also referred to as a polyconjugate polymer. [**20**] Poly(3,4-ethylenedioxythiophene) (PEDOT), polythiophene (PTh), polypyrrole (PPy), polyaniline (PANI), polyvinylpyrrolidone (PVP), polyacetylene (PAC), and so on are the commonly recognized conducting polymers. [**19**]

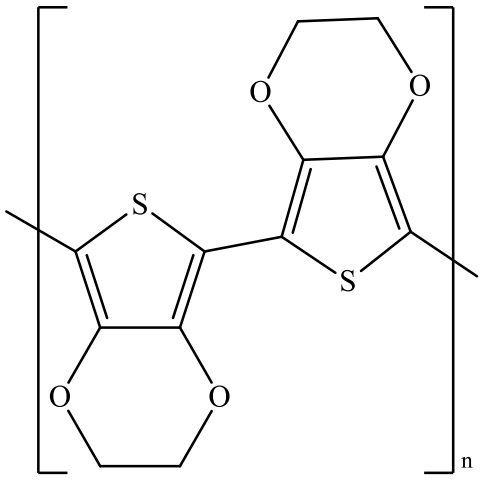

Figure 10: Structural diagram of PEDOT

One of the most extensively used conductive polymers is PEDOT. It is produced from 3,4-ethylenedioxythiophene (EDOT), a monomer. PEDOT is a conjugated polythiophene derivative with a positively charged backbone that contributes to its remarkable oxidative stability and strong electrical conductivity. These approaches make it the most promising material for supercapacitor applications. **Figure 10** shows the structure of PEDOT. [**21**]

There are two types of positions in the thiophene ring of PEDOT structure – 2,5 (α-positions) and 3,4 (β-positions). 2,5 (α-positions) also known as the active site. This position is left open to

connect with other EDOT molecules and intends to form a long polymer chain. This polymerization occurs through the oxidative coupling, which helps to create a linear π-conjugated backbone. Due to this position, charge delocalization occurs. In simple words, electrons flow efficiently through the structure without any obstacles. This efficient charge delocalization characteristic makes PEDOT a good conductive material. [**22**]

A special functional group – ethylenedioxy (–O–CH_2–CH_2–O–) is placed at 3,4 (β-positions) in the thiophene ring of PEDOT. This position provides a special feature to PEDOT, making the structure more stable. Doping or carrying an electric charge can make the PEDOT unstable. However, electrons around the oxygen atom, which belongs to the ethylenedioxy group, help distribute the extra charge properly across the thiophene ring structure. As a result, PEDOT becomes more stable. [**22**]

Except for these two positions in the thiophene ring of PEDOT, it also has two well-recognized resonance structures – benzoid and quinoid. The benzoid structure has a Cα=Cβ bond. This bond contains two conjugated π electrons. On the other hand, the quinoid structure has a Cα–Cβ bond, which lacks the conjugated π electrons like the benzoid structure. This allows the quinoid structure to have delocalized ions. These ions can move freely along the polymer chain. Thus, the quinoid structure of PEDOT makes it more conductive than other polymers. [**23**]

So, due to its special structure, superior stability, and exceptionally high electronic conductivity (values reaching up to 6259S/cm), PEDOT distinguishes itself from other conductive polymers. These attributes have expanded its applicability across flexible and optoelectronic sectors in both industrial and research contexts. [**21**]

1.5. Transition Metal Oxide (MnO2):

In the periodic table, transition metals are those elements which have a partially filled d-orbitals. It includes the elements Ti, V, Cr, Mn, Fe, Co, Ni, Cu, Zn, etc. Transition metals have multiple oxidation states due to the unique nature of their outer d-orbitals. When these metals combine with oxygen, they form transition metal oxides like MnO_2, TiO_2, RuO_2, V_2O_5, Fe_3O_4, and NiO. For supercapacitor applications, these metal oxides are well known as redox/pseudocapacitive materials. [**24**] Therefore, this faradic behavior can provide high theoretical capacitance and fast charge-discharge capabilities in energy storage mechanisms.

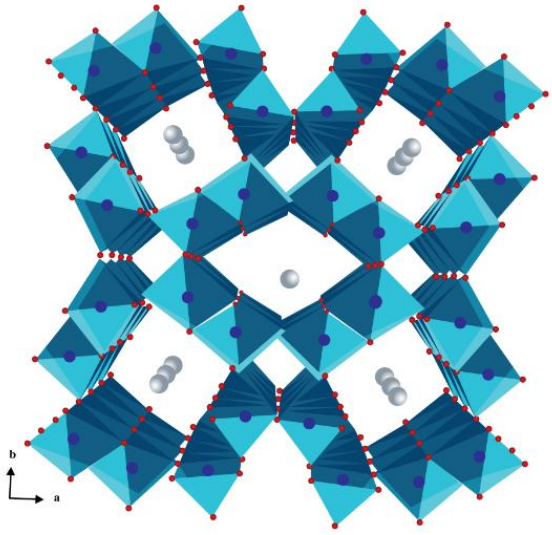

Figure 11: Crystal structure of MnO_2

Manganese, a transition metal, can form multiple oxides, including MnO_2, MnO, Mn_2O_3, and Mn_3O_4, due to its different oxidation states. In supercapacitor application, manganese dioxide is an extensively used electrode material rather than the other manganese oxides. Because of its characteristics, such as availability, minimal toxicity, and eco-friendliness, MnO_2 is widely used. **Figure 11** demonstrates the crystal structure of MnO_2. It has a high theoretical capacitance of approximately 1380 F/g. [**25**] Two reversible redox reactions occur in manganese dioxide-based electrodes, and this is the reason energy can be stored in a pseudo-capacitive manner. This process involves adsorption or desorption of electrolyte cations onto the electrode surface. The oxidation state of manganese can be changed between III and IV during the reaction.

$MnO_2 + M^+ + e^- = MnOOM$

Here, $M = Na^+$ or H_3O^+ [**25**]

1.6. Anionic surfactant (SDS):

An organic compound with non-polar and polar parts is known as a surfactant. It is also referred to as a surface-active agent. The non-polar part typically acts as hydrophobic, and the polar or ionic part acts as hydrophilic. These two parts are positioned at the reverse end of the surfactant molecule. Anionic, cationic, non-ionic, and amphoteric or zwitterionic are several classifications of the hydrophilic part of a surfactant. For example, anionic surfactant includes: sulphonate, sulphate, ether sulphate, ether phosphate ether carboxylate, carboxylate; Cationic includes: primary ammonium, secondary ammonium, tertiary ammonium, quaternary ammonium; Non-ionic includes: polyoxyethylene, monoethanolamine, diethanolamine, polyglucoside; Amphoteric or zwitterionic includes: amine oxide, betaine, amino carboxylates. In contrast, the hydrophobic part includes: alkylbenzene (linear dodecylbenzene), linear alkyl saturated (n-dodecyl), branched alkyl saturated (2-ethylhexyl), linear alkyl unsaturated (oleyl), etc. Wetting ability,

foaming/defoaming, emulsification/demulsification, dispersion, aggregation, solubility, adsorption, micellization, etc. are the identical properties of a surfactant. [**26**]

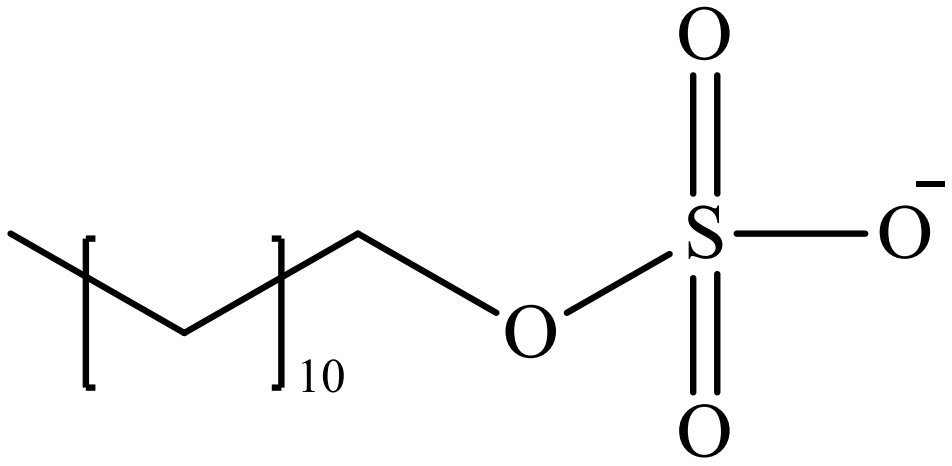

Figure 12: Structural diagram of SDS

Among the anionic surfactants, alkyl sulphate is an important classification on the basis of polymerization application. This alkyl sulphate includes sodium dodecyl sulphate, in short known as SDS. SDS is sodium salt ester of lauryl alcohol/1-dodecanol with C-12. The formula is: $[CH_3(CH_2)10CH_2OSO_3]^-Na^+$

Here,

hydrophobic ion is: CH_3 $(CH_2)10CH_2O$; which is a long hydrocarbon chain that repellant to water.

And hydrophilic ion is: SO_3^- Na^+; with the charge it interacts with water. [**27**] **Figure 12,** represents the structure of SDS.

2. Experimental:

2.1. Literature Review:

Akbar et. el., (2023), activated carbon cloth was used to deposit MnO_2-PEDOT. Pretreatment of activated carbon cloth was done at 400°C. Electrodeposition is a two-step process where MnO_2 is first deposited, followed by PEDOT onto the MnO_2 layer. To deposit MnO_2, with manganese acetate, sodium sulfate solution was used. Additionally, to form the PEDOT layer SDS, and LiCl were used. [**28**]

Lui et. el., (2010) also used a two-step process. In this work, PEDOT nanowires were synthesized initially via electrodeposition. Acetonitrile was used to complete this electrodeposition process. In the second step, PEDOT nanowires were soaked in a $KMnO_4$ solution, leading to the formation of MnO_2 within the PEDOT matrix. [**29**]

Rios et. el., (2011) used a Ti-plate to deposit the composite. Before starting the work, the Ti plate was treated with a hot 10% oxalic acid solution. After that, the composite was deposited in a two-step process. For the electrodeposition of PEDOT, the monomer was dissolved in acetonitrile with $LiClO_4$ as electrolyte. Then $KMnO_4$, an oxidizing agent was used to deposit MnO_2 by over oxidizing the PEDOT. [**30**]

Tang et. el., (2015) used nickel as the working electrode. MnO_2 deposition was the initial process of this three-step methodology. Manganese acetate and sodium sulfate were used to deposit the first layer of MnO_2. As the second part of layer EDOT, SDS and $LiClO_4$ were used to deposit the PEDOT layer on the top of MnO_2. Finally, for the third layer of MnO_2 on top of PEDOT, manganese acetate and sodium sulfate were used. [**31**]

Here, all four works were completed in two or three steps, which is a time-consuming process. In some processes, the working electrode needs a pretreatment. Additionally, all these methods employed multiple starting materials for depositing PEDOT and MnO_2. This was not only time-consuming, but also costly.

2.2. Purpose of the work:

The purpose of this work was to develop an electrode through a single-step fabrication process by combining PEDOT with MnO_2 and to investigate its electrochemical characteristics. MnO_2 used here can significantly influence the charge storage capacity and increase the capacitance. In contrast, PEDOT is well-known for its high electrical conductivity, excellent electrochemical stability, and mechanical flexibility. An anionic surfactant was also used in this process to ensure the homogeneous distribution of the polymer and enhance the adhesion property. The aim of this single-step reaction was to simplify the synthesis process, provide the homogeneous integration of elements, and save both time and cost. This research outcome can contribute to next-generation energy technology by taking a step forward with sustainable electrode materials.

2.3. Materials:

Graphite foil (GF) was sourced from Nanografi. Sodium dodecyl sulfate (SDS), EDOT, manganese acetate, and sodium sulfate were purchased from Sigma-Aldrich.

2.4. Synthesis of Electrodes:

The GF was precisely cut into a 1×4 cm^2 area. It was then mechanically abraded with fine-grade sandpaper to achieve a uniform, roughened surface. This process effectively increases the surface area and enhances the adhesion property. The substrates were then meticulously cleaned by rinsing them with ethanol to ensure the removal of any residual particles and contaminants. In the electrochemical deposition process, the electrolyte solution was prepared by dissolving SDS at a concentration of 0.14 M, along with EDOT and manganese acetate, both at a concentration of 0.08 M, in distilled water in a reaction bottle. To achieve a uniform mixture, the solution was subjected to sonication for 15 minutes before proceeding with the electrochemical deposition. This step was

essential for achieving an even distribution of the monomer and metal within the electrolyte medium. **Figure 13 (a) and (b)** present the synthesis process and electrochemical process for PEDOT-MnO_2 nanocomposite.

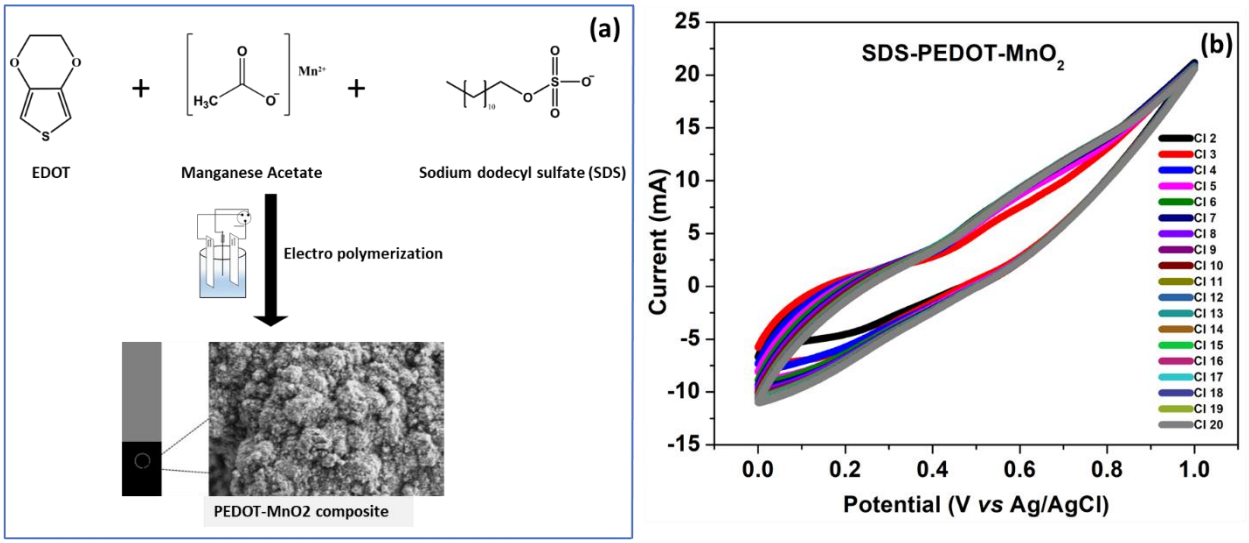

Figure 13: (a) synthesis process diagram of PEDOT-MnO_2 (b) electrochemical synthesis CV curve of PEDOT-MnO_2

The electrochemical deposition was performed using a three-electrode cell configuration. In this arrangement, previously polished GF functioned as the working electrode, a non-polished GF was utilized as the counter electrode, and an Ag/AgCl wire served as the reference electrode. The electrochemical process was facilitated through CV, in a potential window of 0 to 1 V versus Ag/AgCl at a scan rate of 50 mV/s, conducted over 20 cycles. Following the deposition, the electrodes were carefully removed from the electrolyte solution and thoroughly rinsed with distilled water to remove unreacted starting materials. The samples were dried overnight at 70˚C and stored at room temperature until further use.

To ensure the composite formation and compare the electrochemical performance, individual MnO_2 and PEDOT electrodes were made by following the same process as PEDOT-MnO_2 nanocomposite. For these individual electrodes, the electrochemical deposition process was done using CV followed by the same scan rate, cycles and potential window as composite formation. Besides that, the electrolyte solution was prepared for MnO_2, by dissolving SDS at a concentration of 0.14 M, along with manganese acetate (0.08 M), in distilled water within a reaction bottle. In contrast, for PEDOT, the electrolyte solution was prepared by dissolving SDS at a concentration of 0.14 M in distilled water, and EDOT monomer (0.08 M) was added to this solution. To achieve a uniform mixture, both of the individual solutions were subjected to sonication for 15 minutes before proceeding with the electrochemical deposition. **Figure 14 (a), (b)** presents the synthesis process and electrochemical process for individual MnO_2, and **Figure 14 (c), (d)** presents the synthesis process and electrochemical process for individual PEDOT.

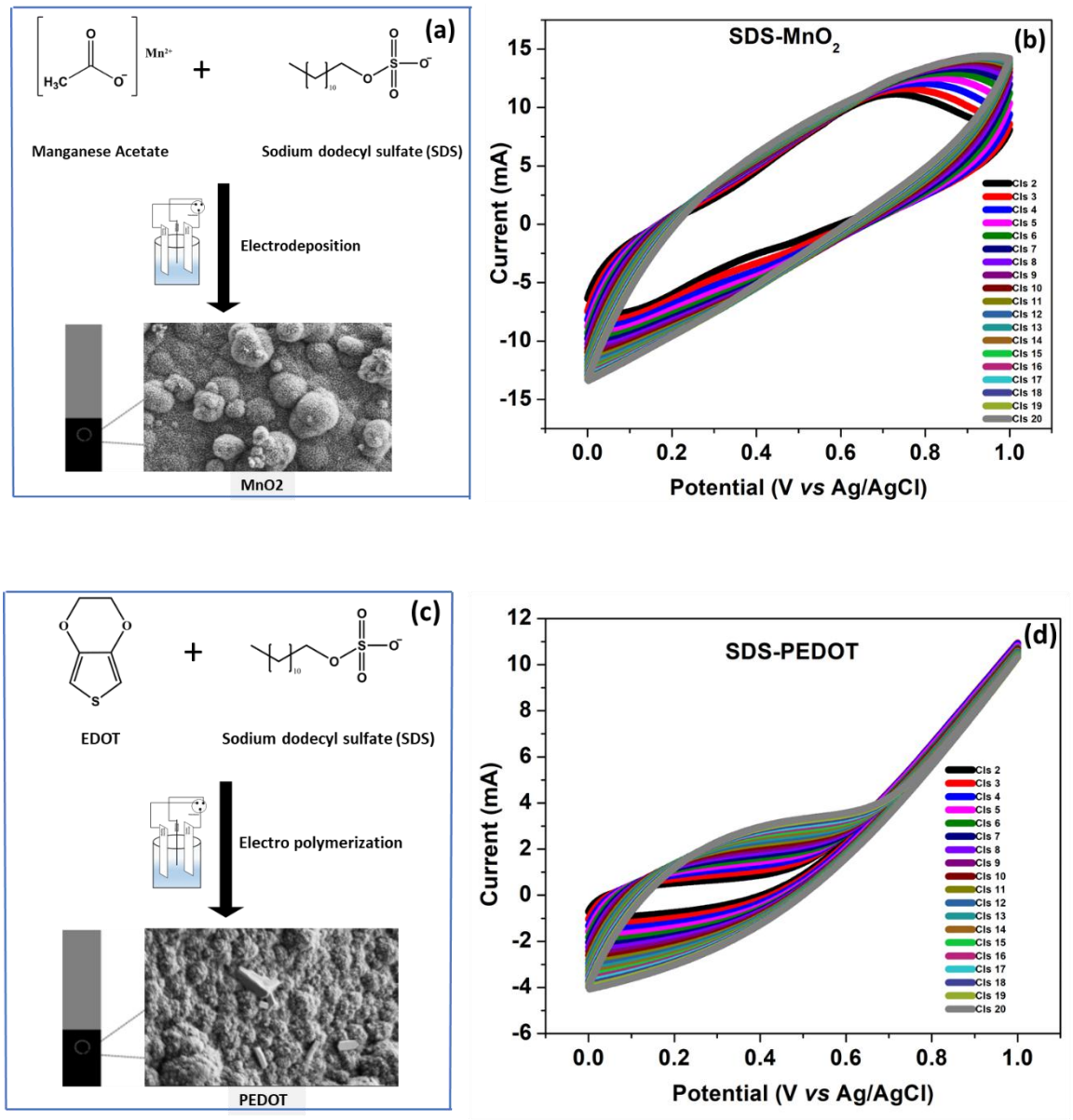

Figure 14: (a) synthesis process diagram of MnO_2 (b) electrochemical synthesis CV curve of MnO_2 (c) synthesis process diagram of PEDOT (b) electrochemical synthesis CV curve of PEDOT-MnO_2

2.5. General Characterization:

To study the molecular vibration and rotation modes, Raman spectroscopy is used as a characterization method. In this analysis process, a distinct spectrum can be found for each molecule. This spectrum can reveal the chemical structure and the composition of a molecule. Chemical bonds in a molecule are excited using a laser of a particular wavelength. Each peak corresponds to the specific Raman shift of a bond in a molecule. [**32**] In this work, Raman

spectroscopy measurements were conducted to provide further insights into the molecular structure and bonding characteristics of the samples.

The characterization method used to identify functional groups is known as Fourier-Transmission Infrared spectroscopy (FTIR). Chemical reaction nature and the classification of a compound can be identified by the functional groups. It is also a quantitative type method, and can be performed on solids, liquids, or gases. When an infrared light is transmitted through the sample, it absorbs some portion of that light. Then, this absorption is measured by the FTIR spectrophotometer. This is the principle of the FTIR method. [**32**] In this study, FTIR spectra were employed to identify the functional groups present in PEDOT, MnO_2, and their composite materials. The FTIR spectra were recorded using a Bruker spectrometer across a wavelength range 400 to 4000 cm^{-1}.

For morphological characterization, the basic method used is known as Scanning Electron Microscopy (SEM). Optical microscopes and SEMs operate in a similar manner. But the main difference between them is instead of light, electron beam is used in SEM analysis. Emission of secondary electrons occurs, when electrons from a beam are directed to the sample. A director then gathers those electrons and generates a morphological image of that sample. [**32**] For this research, surface morphology and microstructural features were examined using a Thermo scientific Apreo Scanning electron microscope (SEM), offering high resolution imaging of the electrode materials used in this work.

2.6. Electrochemical Characterization:

Electrochemical measurements were conducted in a symmetrical three-electrode configuration using 1 M Na_2SO_4 solution as the electrolyte. All measurements were performed using an IviumStat Potentiostat. Before each experiment, the electrodes were saturated by performing 60 cycles at a scan rate of 50 mV/s.

CV measurements were subsequently conducted at seven different scan rates: 10, 20 30, 50, 100, 150, 200 mV/s, within a potential window –0.5 to 0.5 V. For each scan rate five consecutive cycles were recorded, with the fourth cycle selected for analysis and graphical representation to minimize the influence of transient effects and achieve consistent comparisons.

GCD tests were performed under the same electrolyte conditions. The applied current densities ranged from 1 to 10 mA/cm^2, with specific measurements taken at 1, 2, 3, 4,5, 6, 8, and 10 mA/cm^2. These measurements were used to evaluate the rate capability and capacitive behavior of the electrode materials.

EIS measurement was performed to evaluate the interfacial charge transfer resistance, ion diffusion behavior, and overall electrochemical characteristics of the electrode materials. The impedance spectrum was recorded over a frequency range spanning from 1 MHz to 0.1 Hz, with an AC amplitude of 0.01 V. This frequency window was selected to capture both high-frequency processes (such as charge transfer and internal resistance) and low-frequency phenomena (such as ion diffusion and capacitive behavior).

3. Result and Discussion:

3.1. Raman Spectroscopy:

Approximately 574 and 643 cm^{-1} are the two strong characteristic peaks of MnO_2 in Raman spectroscopy (**Figure 15 (a)**). The peak ~574 cm^{-1} is attributed to the Mn–O symmetrical vibration (also referred to as Ag mode in Raman). It suggests the robust tetragonal structure of MnO_2, including an interstitial area with 2 × 2 tunnels. In addition, inside the tetragonal hollandite-type framework, the breathing vibration of MnO_6 octahedra is the reason for the peak at ~643 cm^{-1}. [**33**] The one-dimensional tunnels, which stretch along the spatial axis with a lattice period and a structure of a tetragonal symmetry are known as a hollandite-type framework. Double chains of metal–oxygen octahedra, which are edge-shared with surrounding chains, are the reason for this structure. Therefore, both of the Raman bands discussed here confirm the crystal structure as α-MnO_2. [**34**]

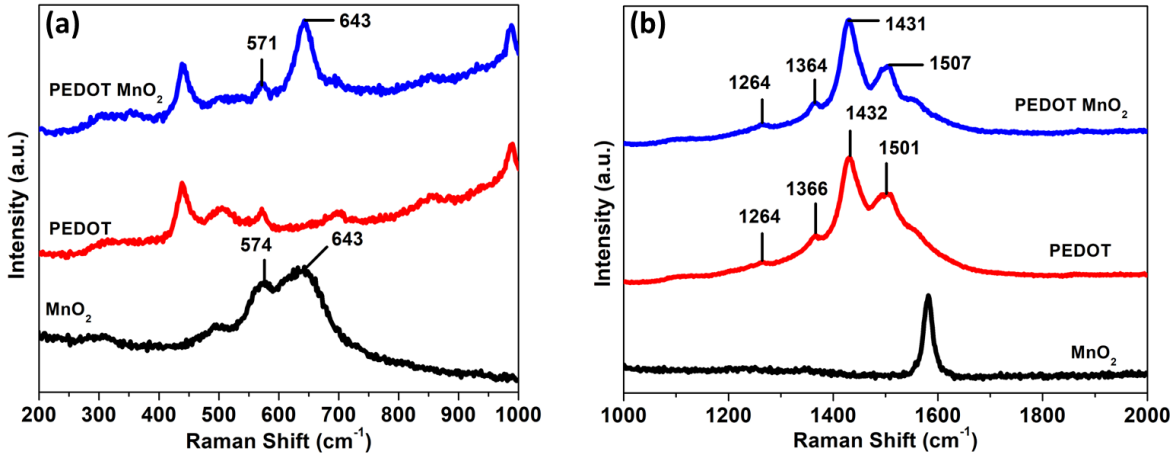

Figure 15: (a) Raman spectra comparison of MnO_2 and PEDOT- MnO_2 (b) Raman spectra comparison of PEDOT and PEDOT- MnO_2

In the Raman spectroscopy of PEDOT (**Figure 15 (b)**), the Cα=Cβ(–O) symmetric stretching vibration is attributed to the intensive peak at ~1432 cm^{-1}. In contrast, Cα=Cβ asymmetric stretching vibration is associated with the peak at ~1501 cm^{-1}. [**35**] This peak corresponds with the thiophene rings in the PEDOT chain. Cβ–Cβ stretching corresponds to the peak at ~1366 cm^{-1}. Along with this, ~1264 cm^{-1} peak was observed for the Cα–Cα inter-ring stretching. [**36**]

In PEDOT-MnO_2 composite, the characterization peak at ~571 cm^{-1} is attributed to the Mn–O symmetrical vibration, which is slightly shifted from the MnO_2. The other peak at ~643 cm^{-1} becomes sharper than the band for pristine MnO_2. This indicates the enhanced structural order and the perfect interaction between the PEDOT polymer and MnO_2. In addition, the characteristic peaks of PEDOT appeared in the composite as slightly shifted with peaks at approximately 1264 cm^{-1}, 1364 cm^{-1}, 1431 cm^{-1}, and 1507 cm^{-1}. It also indicates the structural interactions between PEDOT and MnO_2, confirming the successful formation of the composite.

3.2. FTIR analysis:

The FTIR spectra in **Figure 16** presents the comparative analysis of MnO_2, PEDOT and PEDOT-MnO_2 composite. The sharp peaks at 1618 cm^{-1} and 1107 cm^{-1} correspond to the O-H bond with the Mn atom. These peaks represent the absorbed water. **Figure 16** shows two characteristics peaks at 735 cm^{-1} and 507 cm^{-1}, corresponding to the Mn-O bond vibration. It indicates of α-MnO_2, which originates from the Mn-O bond vibration of MnO_6 octahedra. [**37**]

The distinct characteristics peaks for PEDOT (**Figure 16**) represent the polymer backbone and side groups. The peaks observed at 1560 cm^{-1} and 1464 cm^{-1} correspond to the C=C asymmetric and C-C stretching bonds of the thiophene ring. The peaks for C-O-C stretching in the ethylenedioxy group are observed at 1264, 1161, and 1065 cm^{-1}. Characteristic peaks at 995, 870, and 649 cm^{-1} are attributed to C-S vibrations within the thiophene ring. [**37**]

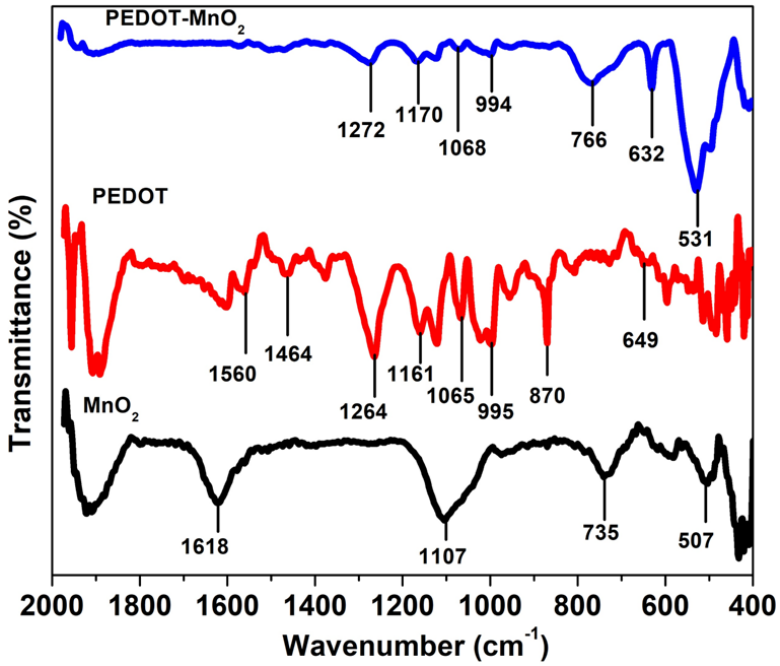

Figure 16: FTIR spectra comparison of PEDOT- MnO_2, PEDOT, and MnO_2

The PEDOT-MnO_2 composite distinctively reveals most of the absorption peaks (**Figure 16**) that are characteristic of both MnO_2 and PEDOT. However, there are some minor shifts and changes in the Mn-O, C-O-C, and C-S bond regions. For example, Mn-O peaks (766 and 531 cm^{-1}) in the composite shifted slightly compared to MnO_2. The O-H bond with the Mn atom, which reveals the absorption of water at the composite, disappears in the composite. In addition, the characteristic peaks for the C-O-C bond of the ethylenedioxy group appear at 1272, 1170, and 1068 cm^{-1}, and the C-S bond of the thiophene ring at 994, 766, and 632 cm^{-1}. These peaks in the composite not only shifted, but also became broader than they appear at PEDOT. Perhaps it occurs due to the strong interfacial interactions between MnO_2 and PEDOT during electrochemical reactions. This interaction demonstrates the successful formation of the composite. [**37**]

3.3. SEM analysis:

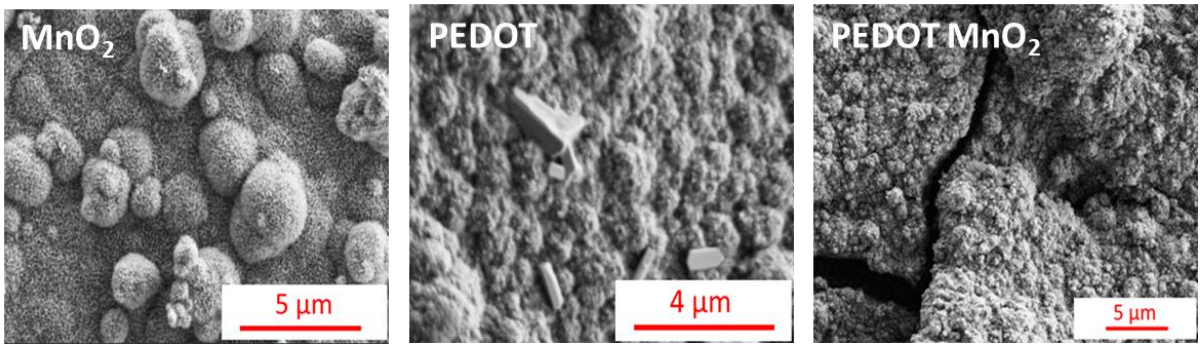

Figure 17: SEM images of MnO_2, PEDOT, and MnO_2-PEDOT composite

SEM was used to analysis the surface morphology of MnO_2, PEDOT and PEDOT-MnO_2 composite as shown in **figure 17**. From the SEM image, MnO_2 looks like a sea-urchin; multiple straight and fast-growing nanorods are the reason for this sea-urchin-like morphology. [**38**] PEDOT shows globular-cluster-like morphology in SEM image analysis. With the increase of PEDOT thickness on electrodes, this globular cluster tends to become bigger. [**39**] When PEDOT and MnO_2 combine, the resulting morphology likely appears as a rough, interconnected granular surface.

3.4. Impact of SDS on electro-polymerization:

Since the PEDOT lacks strong polar functional groups in its structure, it exhibits minimal interactions with water. Due to this poor solubility, SDS was added to water before the EDOT. With a hydrophobic carbon tail, and hydrophilic sulfate head SDS molecules can self-assemble into micelles. Hydrophobic polymer chains like PEDOT can be encapsulated by these micelles. It helps the polymer disperse properly in water and also prevents unwanted polymer aggregation. This results in an increase in the surface morphology by distributing the nanoparticles homogeneously on the electrode surface. [**40**] However, further research is required to clarify the precise effect of SDS on the PEDOT-MnO_2 composite.

3.5. Electrochemical behavior:

3.5.1. Cyclic voltammetry (CV):

To study the redox reaction of electrode-active materials, a fundamental characterization method is employed. This method is referred to as cyclic voltammogram (CV). When a certain scan rate is applied within a given potential window, a current response is recorded in the CV. The relationship between these applied potentials (X-axis) and the corresponding current (Y-axis) is represented through the CV curve. The amount of charge present in the electrode material can be measured by the area of the CV curve. Besides, specific capacitance, power density, and energy density can be calculated from this curve. [**21**]

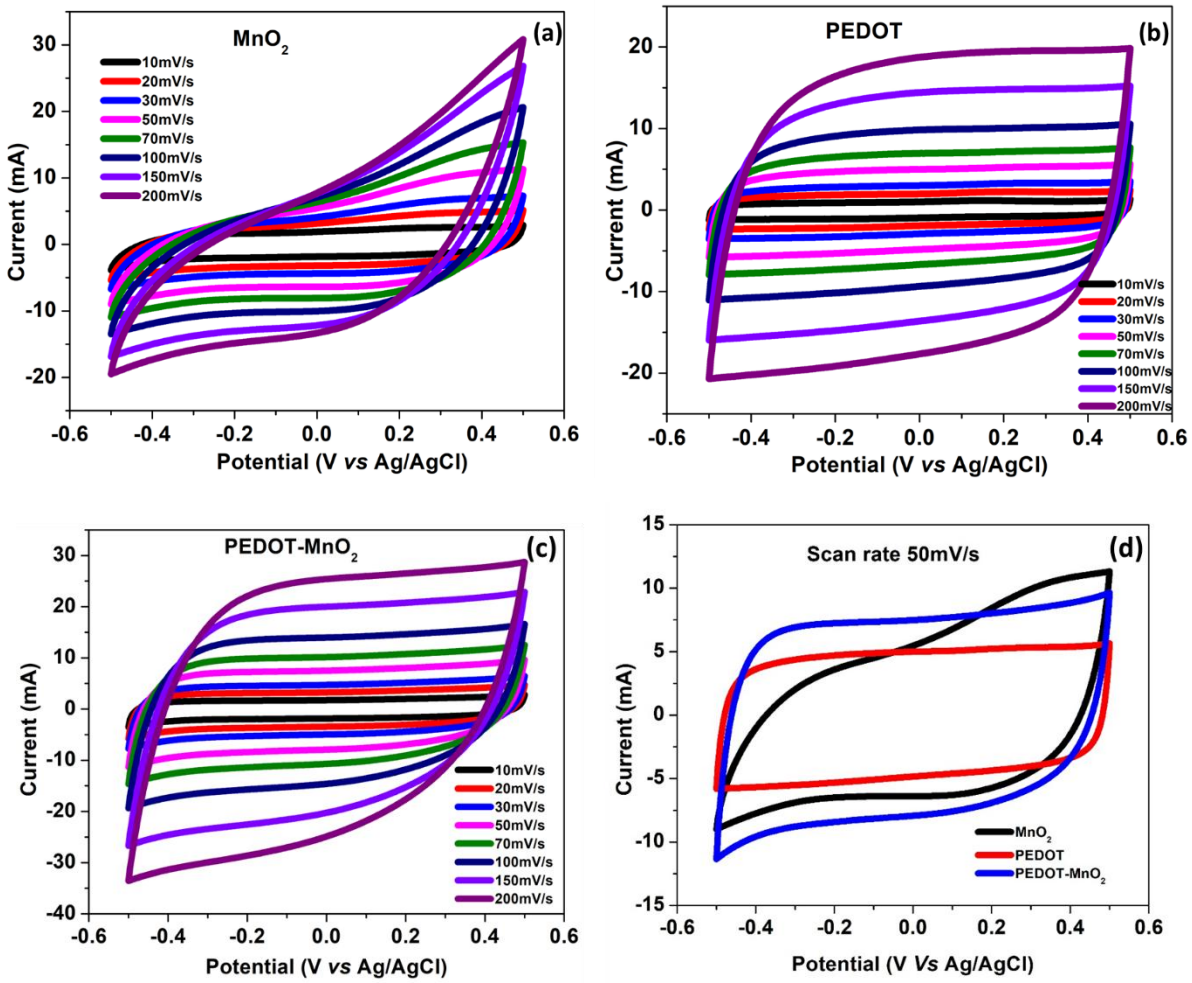

Figure 18: (a) CV curve of MnO_2 at different scan rates (b) CV curve of PEDOT at different scan rates (c) CV curve of PEDOT-MnO_2 composite at different scan rates (d) CV performance comparison at scan rate 50mV/s

The current vs potential graph of MnO_2 is demonstrated in **figure 18 (a)**. This graph displays the current response data at different scan rates, ranging from 10 mV/s to 200 mV/s. MnO_2 is a pseudo capacitive material. This type of material makes a quasi-rectangular shape during the CV measurement graph. This shape is a cause of surface or near-surface redox reactions. When the electrolyte ions completely penetrate the electrode structure, they can participate in this redox reaction. This whole process is possible at a low scan rate, when the ions get enough time to diffuse. But the scenario becomes completely reversed if the scan rate increases. Because then ions cannot get enough time to speed up the surface reaction kinetics. So, CV curves become distorted from the ideal shape of a pseudo capacitive material. [**41**]

Figure 18 (b) shows the CV curve for PEDOT at different scan rates ranging from 10 mV/s to 200 mV/s. The shape of this curve at a lower scan rate is almost rectangular. This is also a common structure for EDLC capacitance. In this mechanism an electrostatic reaction is responsible for storing energy. However, a minimal involvement of the faradic reaction can be observed. In this reaction mechanism, the charge is stored through ion accumulation which occurs at the electrode-

electrolyte interface. So, the fast and reversible adsorption or desorption of ions at a lower scan rate is the reason for the rectangular shape of the CV in PEDOT. However, like MnO_2 a slight distortion occurs with increasing scan rate. The main cause here is the limitation of the ion kinetics. [**42**] The PEDOT-MnO_2 CV curve is shown at **figure 18 (c)**. Here, the CV curve is also almost rectangular at a lower scan rate, but it distorts as the scan rate increases.

A standard scan rate of 50 mV/s was selected to analyze the comparable electrochemical performance of MnO_2, PEDOT, and the PEDOT-MnO_2based composite. **Figure 18 (d)** shows the comparison. The CV curve of the composite shows an increased charge storage capacity compared to the individual components of PEDOT and MnO_2. This is due to the synergistic interaction of both molecules, which is reflected in an excellent current response and a larger CV curve area than the individual MnO_2 and PEDOT.

3.5.2. Galvanostatic charge-discharge (GCD):

Galvanostatic charge-discharge (GCD) is a method to measure the cyclic stability of an electrode. In this process, potential variation is recorded over time at a constant current. In the GCD curve, the X- axis is set as potential and Y-axis is set as time. If the curve shape is triangular, it indicates the EDLC materials, such as PEDOT. If the shape is non-triangular, it can be a pseudocapacitive material, like MnO_2. [**21**]

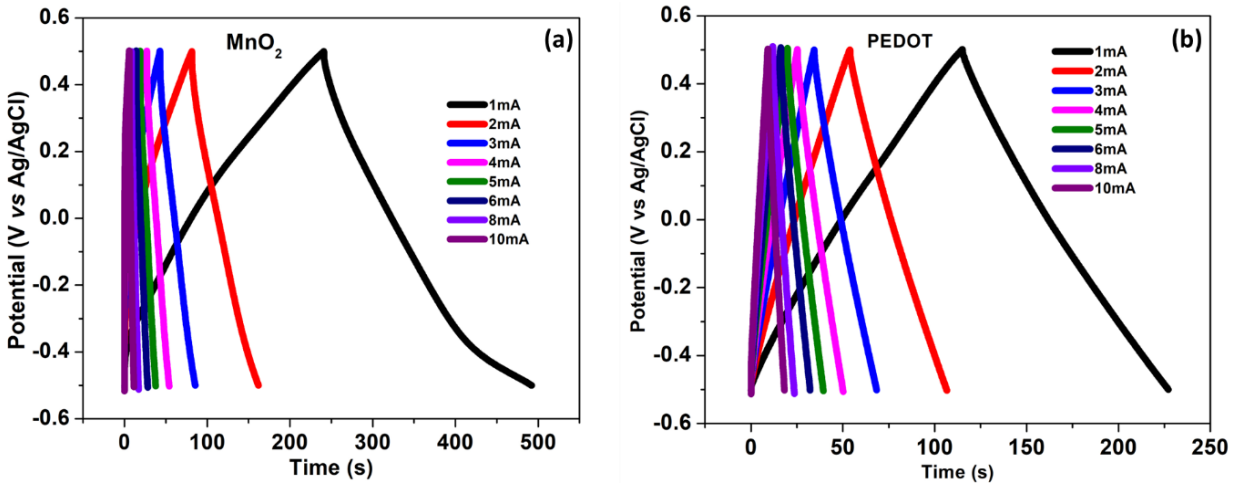

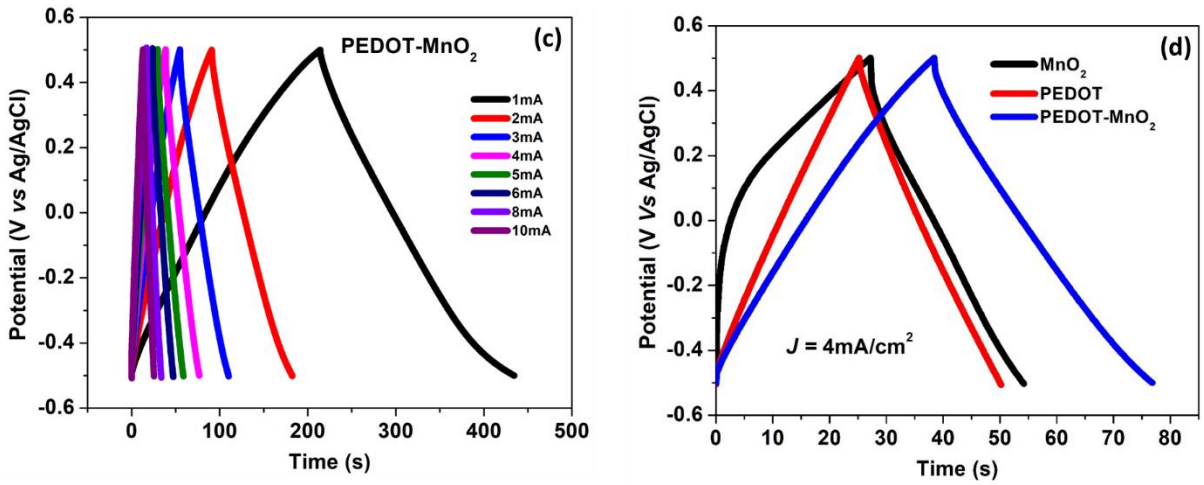

Figure 19: (a) GCD curve of MnO_2 at different currents (b) GCD curve of PEDOT at different currents (c) GCD curve of PEDOT-MnO_2 composite at different currents (d) GCD performance comparison at 4mA/cm^2

At **Figure 19 (a), (b), (c)**, the GCD curve represents the recorded electrochemical response of MnO_2, PEDOT and PEDOT-MnO_2 composite, respectively, during the charge-discharge process. Here, the discharging time decreases with the increase of the constant current. For example, at 1mA current, the MnO_2, PEDOT, and PEDOT-MnO_2 composite showed higher discharge times – around 500, 240, and 450 seconds, respectively. However, at higher currents, such as 10 mA, the discharge time becomes faster, indicating a reduction in energy storage per cycle. **Figure 19 (d)** represents the comparison among the MnO_2, PEDOT and PEDOT-MnO_2 composite of the GCD curve. For this comparison graph, a constant current density of 4 mA/cm^2 was selected for analysis. Here, individual MnO_2 exhibits a non-linear curve of pseudo capacitance character with poor electrical conductivity, and individual PEDOT exhibits a linear curve of EDLC character with lower specific capacitance. When these two combine, PEDOT improves conductivity, and MnO_2 improves capacitance, and resulting in a synergistic effect that improves the charge storage capability of the composite material. The longest discharge time (almost 80s) of the composite is proof of this enhanced performance characteristic.

3.5.3. Electrical impedance spectroscopy (EIS):

EIS spectroscopy is a frequently used method for energy storage devices. It can offer mechanical and kinetic data. When the electrochemical system is in a steady state or under equilibrium, a minimal amount of alternating current (AC) or voltage is applied over an extensive range of frequencies. So, a minor disturbance happens in the system. Due to this disturbance, when systems respond as current or voltage, the EIS measures that response to analyze the resistance behavior of the SC. [**21**] There are two types of graphs used in this process analysis: Nyquist plot, and Bode-phase plot. Between them the Nyquist plot is the most standard graph for the EIS technique. This plot represents the relationship between the real part (X-axis) and the imaginary part of impedance

(Y-axis). In contrast, the relationship between phase and frequency represents the Bode-phase plot. [**43**]

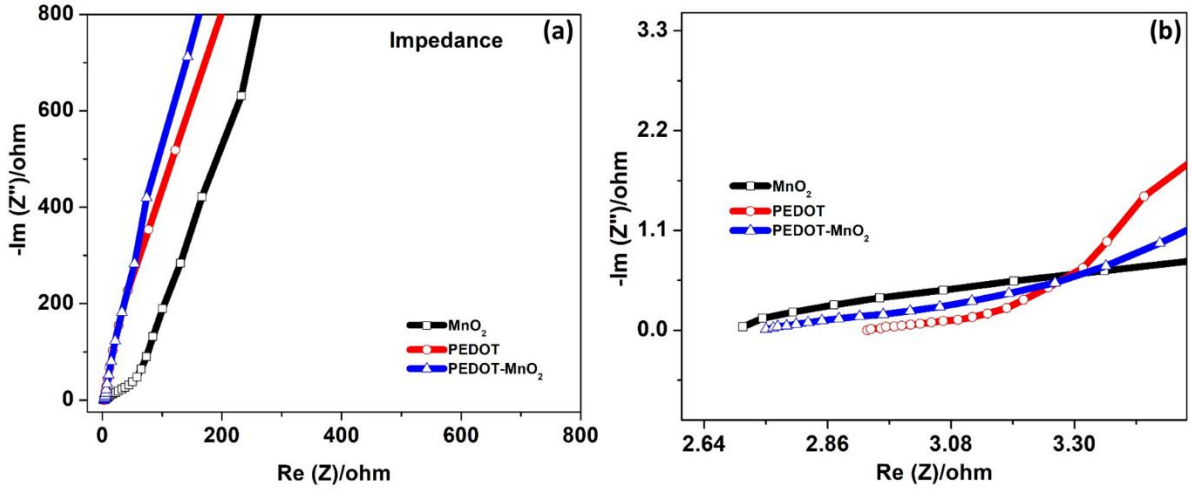

Figure 20: (a) The Nyquist diagram (b) Zoomed view of Nyquist diagram

Figure 20 (a) and (b) represents the same Nyquist plot. Here, **figure 20 (a)** falls within the broader frequency range, and **figure 20 (b)** is a zoomed-in view of the high-frequency region. If the real impedance is high, the material exhibits a high charge transfer resistance (Rct). From **figure 20 (b)**, PEDOT represents a lower Rct value than MnO_2. Therefore, PEDOT is significantly more capable of transferring charge through the electrode and exhibits better conductivity than MnO_2. On the other hand, the PEDOT-MnO_2 composite shows a lower Rct value than MnO_2, but a slightly higher value than PEDOT. This indicates a moderate performance in the fast charge transfer process.

3.5.4. Specific capacitance:

High power providing ability, along with excellent specific capacitance is the key feature of a supercapacitor. In per unit mass, the amount of charge that electrode material can hold is called the specific capacitance. To find the effectiveness of a component that is employed in a charge storage device, specific capacitance is important as a performance assessing parameter. The following formula is used to determine it from GCD data,

specific capacitance = $(I \times \Delta t)/ (\Delta V \times a)$

Here,

Discharge current = I (A)

Discharge time = Δt (s)

Potential window = ΔV (V)

Area of the active materials = a (cm^2)

The specific capacitance can be influenced by two different parameters: measurement and intrinsic or fundamental properties. Testing methods, electrodes, and the configuration of testing cells are part of the measurement, while morphologies, crystal structures, electrochemical activity, and charge–discharge mechanisms are part of the intrinsic properties.

Due to the lack of an established or stable chemical formula, MnO_2 represents a complicated form of inorganic metal oxide. Through van der Waals force – water molecules, foreign atoms like Na^+, K^+, and vacancies may be retained in its crystal structure. The arrangement of manganese and oxygen within the lattice can form some open pathways, which are referred to as tunnels. These tunnels allow the mobility of ions, which leads to the accumulation of the electrical charge. For instance, α–MnO_2 has a (2×2) tunnel structure, and λ–MnO_2 has a 3D tunnel network. In comparison to λ–MnO_2, α–MnO_2 demonstrates the superior specific capacitance. [**44**] Based on the **figure 21 (a)**, the MnO_2 electrode demonstrates a specific capacitance of around 255 $mFcm^{-2}$ at a current range of 1 mA, which is higher than PEDOT itself and the PEDOT–MnO_2 composite. The pseudo capacitance characteristics of MnO_2 are the reason for this high capacitance. At lower current densities, electrolyte ions have enough time to activate the redox sites for maximum use. It happens due to the complete diffusion of ions into the structure, which increases the specific capacitance value. In contrast, redox reactions occur at the outer surface due to the limitation of ion diffusion. This occurs with the rise in current density (10 mA), and the capacitance drops by almost 74%.

Remarkable structural stability and excellent electrical conductivity are two renowned characteristics for a π–conjugated polymer like PEDOT. According to the **figure 21 (a)**, it shows a specific capacitance of 113 $mFcm^{-2}$ at a 1 mA current density. This value is lower than the MnO_2 alone or the composite of MnO_2-PEDOT. But within the increasing current density, instead of dropping the capacitance value remains nearly stable. For example, at a 10mA current density, the capacitance value was 95 $mFcm^{-2}$. Rather than pseudo capacitive redox reactions, it operates through an EDLC mechanism. In this mechanism, ion adsorption at the electrode–electrolyte interface facilitates charge storage. It has a low surface area due to its tightly confined and compact morphology. The quantity of the electrochemically active sites for ion adsorption becomes limited due to this morphology. Along with this, the charge storage capacity and capacitance value drop by around 16% of the other elements in **figure 21 (a)**. But the advantages of PEDOT include structural stability and rigidity. Even during the continuous charge–discharge cycles it can maintain these characteristics. Consequently, despite showing a low capacitance value, it can guarantee a stable capacitance, due to its durable characteristics. [**22**]

Thus, to enhance the specific capacitance and stability, MnO_2 and PEDOT are combined together. Due to this synergistic effect, the specific capacitance of this composite reaches 222 $mFcm^{-2}$ at a 1 mA current density and remains almost stable (137 $mFcm^{-2}$) until the current density reaches 10 mA. This indicates that the composite not only exhibits high capacitance values comparable to those of MnO_2 and PEDOT, but also maintains good rate performance (almost 61%), further confirming the synergistic effect of both components in the composite.

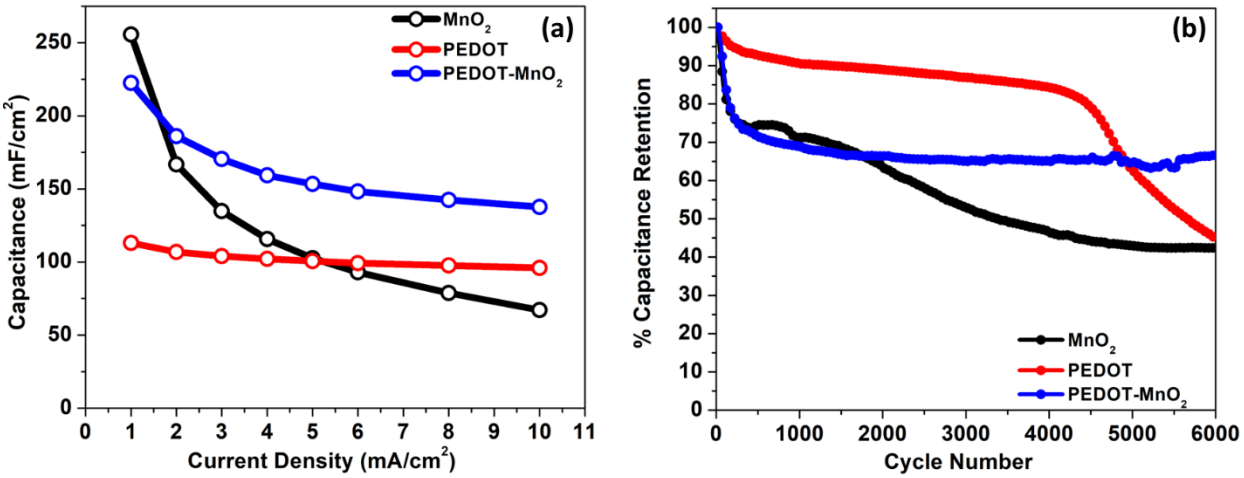

Figure 21: (a) Capacitance comparison, (b) Cycling performance

3.5.5. Cycling stability:

During a frequent charge-discharge cycle, the ability to retain the stored capacity is referred to as capacitance retention. [**45**] **Figure 21 (b)** demonstrates the cycling performance comparison among the MnO_2, PEDOT, and MnO_2-PEDOT composite. Among these three materials, PEDOT shows the best cycling stability up to 4500 cycles, with capacitance retention of 85%. After 4500 cycles, the material started to degrade, and at 6000 cycles, the capacitance decreased to below 50%. From the start of the cycles, MnO_2 showed inadequate stability and it continued to degrade until 6000 cycles. The capacitance retention value was around 45% after 6000 cycles. However, the PEDOT-MnO_2 composite showed a capacitance retention value of more than 65% at 1000 cycles. This capacitance was maintained for 6000 cycles, the highest among all three materials. This characterization established the advantages of the synergistic effect of PEDOT-MnO_2 composite during the long-term charge-discharge process and ensured its long lifespan.

3.5.6. Effect of electrolytes:

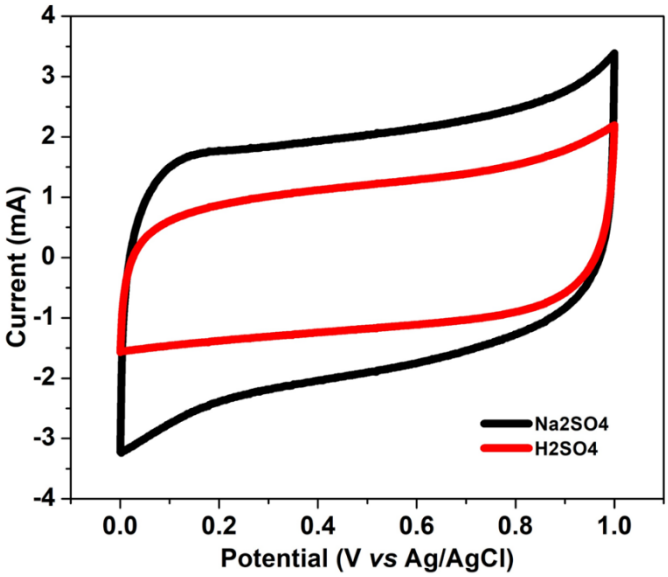

Figure 22: Electrochemical performance (CV) comparison of PEDOT-MnO_2 composite in Na_2SO_4 and H_2SO_4 electrolyte

The Na_2SO_4 electrolyte shows (**Figure 22**) an almost rectangular CV curve, indicating its EDLC characteristics. It also exhibits a higher current value (more than 3mA). It implies enhanced charge accumulation and superior capacitive performance of the electrode in a Na_2SO_4-based electrolyte.

On the other hand, the H_2SO_4 electrolyte also shows a nearly rectangular CV curve, similar to that of the Na_2SO_4 electrolyte. But it has a lower current value of around 1.5 mA. In comparison with the Na_2SO_4 electrolyte, this indicates inferior ion diffusion kinetics.

4. Future prospects:

This research focuses on the synthesis of PEDOT-MnO_2 based nanocomposites with a surfactant SDS. For this work a specific equal ratio of PEDOT and manganese acetate was used. In the future, optimizing the ratios of the starting materials could enhance the double layer capacitance and pseudo capacitance behavior. Except Na_2SO_4, other types of electrolytes, such as H_2SO_4, and $NaClO_3$ can be used to achieve an enhanced voltage window range. X-ray diffraction (XRD) and transmission electron microscopy (TEM) are advanced techniques that need to be employed. To understand the relation between the structure and performance of materials, these characterization processes will provide comprehensive structural and crystallographic data. To evaluate more accurate electrochemical performance under actual circumstances, a two-electrode setup must be used instead of a three-electrode system.

5. Conclusion:

This study represents the successful formation of PEDOT-MnO_2 based nanocomposites through the electrochemical deposition process. The objective of this work was to reduce the reaction time by depositing the MnO_2 and PEDOT simultaneously in a one-pot synthesis. It is a simple, single-step process, employing SDS as a surfactant, which ensures the homogeneous distribution of the polymer on the surface and improves adhesion to the electrodes. 1M Na_2SO_4 was used in this research as a neutral electrolyte to achieve enhanced cycling stability and capacitance values. It also helps in fast and efficient ion diffusion. PEDOT is well known as a highly electrically conductive material. In contrast, MnO_2 is prominent for high theoretical capacitance. To prove the perfect combination of these two materials, electrochemical characterizations processes, such as CV, CD, and impedance were performed. In CV characterization, the nanocomposite showed the highest current response, a larger CV area, and an almost ideal rectangular shape, which proves its excellent capacitive behavior. GCD curves demonstrate the longest discharge time even at the highest current density, which also helps to calculate the specific capacitance. PEDOT-MnO_2 nanocomposite exhibited highest specific capacitance around 222 mF/cm^2 at 1 mA/cm^2 and around 137 mF/cm^2 specific capacitance at 10 mA/cm^2. Whereas individual MnO_2 and PEDOT showed the highest values of 255 mF/cm^2, 113 mF/cm^2, respectively, and the lowest values of around 67 mF/cm^2, and 95 mF/cm^2 respectively. These values emphasize the higher capacitance stability of the developed composite material. Although initially the composite was initially unable to achieve stable capacitance retention compared to individual PEDOT, after 1000 cycles, it became stable. This indicates the synergistic combination of PEDOT and MnO_2 can improve cycling stability compared to the individual components. All these characterizations are performed on the composite material, demonstrating the enhancement of capacitive behavior achieved by integrating the conductive polymer and transition metal oxide. This study highlights the pathway for utilizing this electrode in supercapacitor-type energy storage applications. In addition, this can also serve as a good example of an economically viable and time-saving process.

6. Acknowledgement:

All the figures draw by Adobe Photoshop, ChemDraw, and Origin.

7. References:

[1] IEA (2025), Global Energy Review 2025, IEA, Paris https://www.iea.org/reports/global-energy-review-2025, Licence: CC BY 4.0

[2] Ritchie, H., Rosado, P., & Roser, M. (2020). Breakdown of carbon dioxide, methane and nitrous oxide emissions by sector. Our World in Data.

[3] Vision, I. C. C. T. (2020). 2050-a strategy to decarbonize the global transport sector by mid-century. International Council on Clean Transportation.

[4] Zhang, J., Gu, M., & Chen, X. (2023). Supercapacitors for renewable energy applications: A review. Micro and Nano Engineering, 21, 100229.

[5] Olabi, A. G., Abbas, Q., Al Makky, A., & Abdelkareem, M. A. (2022). Supercapacitors as next generation energy storage devices: Properties and applications. Energy, 248, 123617.

[6] Kim, B. K., Sy, S., Yu, A., & Zhang, J. (2015). Electrochemical supercapacitors for energy storage and conversion. Handbook of clean energy systems, 1-25.

[7] Pramitha, A., & Raviprakash, Y. (2022). Recent developments and viable approaches for high-performance supercapacitors using transition metal-based electrode materials. Journal of Energy Storage, 49, 104120.

[8] Xie, J., Yang, P., Wang, Y., Qi, T., Lei, Y., & Li, C. M. (2018). Puzzles and confusions in supercapacitor and battery: Theory and solutions. Journal of Power Sources, 401, 213-223.

[9] https://faculty.kfupm.edu.sa/me/hussaini/corrosion%20engineering/02.05.04.htm

[10] Zoski, C. G. (Ed.). (2006). Handbook of electrochemistry. Elsevier.

[11] Elgrishi, N., Rountree, K. J., McCarthy, B. D., Rountree, E. S., Eisenhart, T. T., & Dempsey, J. L. (2018). A practical beginner's guide to cyclic voltammetry. Journal of chemical education, 95(2), 197-206.

[12] Xu, K. (2004). Nonaqueous liquid electrolytes for lithium-based rechargeable batteries. Chemical reviews, 104(10), 4303-4418.

[13] Béguin, F., Presser, V., Balducci, A., & Frackowiak, E. (2014). Carbons and electrolytes for advanced supercapacitors. Advanced materials, 26(14), 2219-2251.

[14] Iqbal, M. Z., Zakar, S., & Haider, S. S. (2020). Role of aqueous electrolytes on the performance of electrochemical energy storage device. Journal of Electroanalytical Chemistry, 858, 113793.

[15] Banerjee, S., De, B., Sinha, P., Cherusseri, J., & Kar, K. K. (2020). Applications of supercapacitors. Handbook of nanocomposite supercapacitor materials I: characteristics, 341-350.

[16] Sykam, N., Gautam, R. K., & Kar, K. K. (2015). Electrical, mechanical, and thermal properties of exfoliated graphite/phenolic resin composite bipolar plate for polymer electrolyte membrane fuel cell. Polymer Engineering & Science, 55(4), 917-923.

[17] Szubzda, B., Szmaja, A., Ozimek, M., & Mazurkiewicz, S. (2014). Polymer membranes as separators for supercapacitors. Applied Physics A, 117, 1801-1809.

[18] Kouchachvili, L., Yaïci, W., & Entchev, E. (2018). Hybrid battery/supercapacitor energy storage system for the electric vehicles. Journal of Power Sources, 374, 237-248.

[19] Meer, S., Kausar, A., & Iqbal, T. (2016). Trends in conducting polymer and hybrids of conducting polymer/carbon nanotube: a review. Polymer-Plastics Technology and Engineering, 55(13), 1416-1440.

[20] Taherian, R. (2019). The theory of electrical conductivity. Electrical Conductivity in Polymer-Based Composites: Experiments, Modelling and Applications, 1-18.

[21] Thomas, S. A., Cherusseri, J., Baby, A., Rajendran, D. N., Isaac, R., & Kumar, D. (2024). Designing PEDOT-based hybrid electrodes for supercapacitors by electrospinning strategy. DiSCover Electrochemistry, 1(1), 6.

[22] Zhang, T., Wu, J., & Ran, F. (2024). Poly (3, 4-Ethylenedioxythiophene) as Promising Energy Storage Materials in Zinc-Ion Batteries. Macromolecular Rapid Communications, 45(23), 2400476.

[23] Park, J. K., Kang, T. G., Kim, B. H., Lee, H. J., Choi, H. H., & Yook, J. G. (2018). Real-time humidity sensor based on microwave resonator coupled with PEDOT: PSS conducting polymer film. Scientific reports, 8(1), 439.

[24] Rao, C. N. R. (1989). Transition metal oxides. Annual Review of Physical Chemistry, 40(1), 291-326.

[25] Pasierb, P. (2025). Effect of microstructure on performance and working mechanism of MnO2-PEDOT supercapacitors based on nonaqueous electrolytes. Journal of Energy Storage, 106, 114824.

[26] Farn, R. J. (Ed.). (2006). Chemistry and technology of surfactants (No. 272299). Blackwell Pub.

[27] Singer, M. M., & Tjeerdema, R. S. (1993). Fate and effects of the surfactant sodium dodecyl sulfate. Reviews of Environmental Contamination and Toxicology: Continuation of Residue Reviews, 95-149.

[28] Akbar, A. R., Saleem, A., Rauf, A., Iqbal, R., Tahir, M., Peng, G., ... & Liu, F. (2023). Integrated MnO2/PEDOT composite on carbon cloth for advanced electrochemical energy storage asymmetric supercapacitors. Journal of Power Sources, 579, 233181.

[29] Liu, R., Duay, J., & Lee, S. B. (2010). Redox exchange induced MnO2 nanoparticle enrichment in poly (3, 4-ethylenedioxythiophene) nanowires for electrochemical energy storage. Acs Nano, 4(7), 4299-4307.

[30] Rios, E. C., Correa, A. A., Cristovan, F. H., Pocrifka, L. A., & Rosario, A. V. (2011). Poly (3, 4-ethylenedioxithiophene)/MnO2 composite electrodes for electrochemical capacitors. Solid state Sciences, 13(11), 1978-1983.

[31] Tang, P., Han, L., Zhang, L., Wang, S., Feng, W., Xu, G., & Zhang, L. (2015). Controlled Construction of Hierarchical Nanocomposites Consisting of MnO2 and PEDOT for High-Performance Supercapacitor Applications. ChemElectroChem, 2(7), 949-957.

[32] Alqaheem, Y., & Alomair, A. A. (2020). MicroSCopy and spectroSCopy techniques for characterization of polymeric membranes. Membranes, 10(2), 33.

[33] Gao, T., Fjellvåg, H., & Norby, P. (2009). A comparison study on Raman scattering properties of α- and β-MnO2. Analytica chimica acta, 648(2), 235-239.

[34] Fujimoto, K., Takamori, K., Yamaguchi, Y., & Ito, S. (2014). Single crystal growth and structure refinement of hollandite-type K1. 98Fe1. 98Sn6. 02O16. Journal of crystal growth, 390, 88-91.

[35] Xu, B., Gopalan, S. A., Gopalan, A. I., Muthuchamy, N., Lee, K. P., Lee, J. S., ... & Kang, S. W. (2017). Functional solid additive modified PEDOT: PSS as an anode buffer layer for enhanced photovoltaic performance and stability in polymer solar cells. Scientific reports, 7(1), 45079.

[36] Chiu, W. W., Travaš-Sejdić, J., Cooney, R. P., & Bowmaker, G. A. (2006). Studies of dopant effects in poly (3, 4-ethylenedi-oxythiophene) using Raman spectroscopy. Journal of Raman Spectroscopy: An International Journal for Original Work in all Aspects of Raman Spectroscopy, Including Higher Order Processes, and also Brillouin and Rayleigh scattering, 37(12), 1354-1361.

[37] Zhou, H., Zhi, X., & Zhai, H. J. (2018). Promoted super capacitive performances of electrochemically synthesized poly (3, 4-ethylenedioxythiophene) incorporated with manganese dioxide. Journal of Materials Science: Materials in Electronics, 29, 3935-3942.

[38] Feng, L., Xuan, Z., Zhao, H., Bai, Y., Guo, J., Su, C. W., & Chen, X. (2014). MnO 2 prepared by hydrothermal method and electrochemical performance as anode for lithium-ion battery. NanoSCale research letters, 9, 1-8.

[39] Patra, S., Barai, K., & Munichandraiah, N. (2008). Scanning electron microscopy studies of PEDOT prepared by various electrochemical routes. Synthetic Metals, 158(10), 430-435.

[40] Behniafar, H., & Yousefzadeh, D. (2015). Chemical synthesis of PEDOT/Ag nanocomposites via emulsion technique in silver colloid. Designed Monomers and Polymers, 18(1), 6-11.

[41] Jiang, Y., & Liu, J. (2019). Definitions of pseudocapacitive materials: a brief review. Energy & Environmental Materials, 2(1), 30-37.

[42] Liew, C. W., Ramesh, S., & Arof, A. K. (2016). Enhanced capacitance of EDLCs (electrical double layer capacitors) based on ionic liquid-added polymer electrolytes. Energy, 109, 546-556.

[43] Niya, S. M. R., & Hoorfar, M. (2013). Study of proton exchange membrane fuel cells using electrochemical impedance spectroscopy technique–A review. Journal of Power Sources, 240, 281-293.

[44] Yan, J., Sumboja, A., Wang, X., Fu, C., Kumar, V., & Lee, P. S. (2014). Insights on the fundamental capacitive behavior: a case study of MnO2. Small, 10(17), 3568-3578.

[45] Mahala, S., Khosravinia, K., & Kiani, A. (2023). Unwanted degradation in pseudo capacitors: Challenges and opportunities. Journal of Energy Storage, 67, 107558.